Ro-vibrational Population Distribution in the Ground State of Hydrogen Isotopologues in LHD Peripheral Plasmas Deduced from Emission Spectroscopy

Hiroki ISHIHARA, Arseniy KUZMIN, Masahiro KOBAYASHI1, Taiichi SHIKAMA, Keiji SAWADA2, Seiki SAITO3, Hiroaki NAKAMURA1, Keisuke FUJII, Masahiro HASUO, and the LHD Experiment Group1

Graduate School of Engineering, Kyoto University, Kyotodaigaku-katsura, Nishikyo-ku, Kyoto, 614-8540, Japan

1National Institute for Fusion Science, 322-6 Oroshi-cho, Toki, Gifu, 5909-5292, Japan

2Faculty of Engineering, Shinshu University, 4-17-1 Wakasato, Nagano 380-8553, Japan

3Graduate School of Science and Engineering, Yamagata University, Yonezawa,992-8510, Japan

Wide wavelength range with high-resolution emission spectroscopy was applied to LHD peripheral plasmas. All measured Fulcher-*a* band Q-branches spectra (600-630 nm) were measured with a single shot exposure time of 100-200 ms for all investigated discharges. Ro-vibrational populations up to v = 2 and N = 11 for H_2 and up to v = 3 and N = 14 for D_2 in the $3p^3\Pi_u$ state were estimated, where v and N are vibrational and rotational quantum numbers, respectively. It was found that the rotational population of every vibrational state follows two-temperature Boltzmann distribution. From the calculation with a coronal model, ro-vibrational populations distribution up to such high N quantum numbers in the ground state are deduced.

Keywords: Fulcher-*a* band, hydrogen molecule isotope, ro-vibrational population, large helical device

corresponding author: kuzmin.arseniy.6x@kyoto-u.ac.jp

1 Introduction

Hydrogen recycling is one of the main issues in a thermonuclear fusion reactor. Recently, more and more attention is paid to the hydrogen transport in the peripheral region and to plasma-wall interaction, including atomic and molecular hydrogen processes. It has been known that the reaction rate of molecular assisted recombination (MAR) strongly depends on the vibrational and rotational states of hydrogen molecules in the ground state [1, 2]. Recently, vibrational and rotational state distribution of hydrogen molecules emitted from carbon divertor plate has been calculated with molecular dynamics simulation [3]. For the purpose of comparison, experimental data of the population up to high ro-vibrational states in the ground state is demanded. Such data is available for various small-scale laboratory plasmas, i.e. glow and arc discharges with different methods, such as coherent anti-Stokes Raman scattering (CARS) spectroscopy and laser induced fluorescence (LIF) spectroscopy [4, 5]. In these measurements, ro-vibrational population have been evaluated up to high states, $v = 13$ and $N = 11$ for H_2 in [5], $v = 2$ and $N = 17$ for H_2 in [4], where v and N are vibrational and rotational quantum numbers, respectively.

In fusion devices, such direct measurement of the ground state is usually difficult, and the Fulcher-α band emission spectroscopy in the visible range is generally carried out. In this case, however, ro-vibrational populations of the electronically exited state (the $3p^3\Pi_u$ state) of hydrogen molecules are measured; up to $v = 4$ and $N = 8$ in [6] and up to $v = 5$ and $N = 15$ in [7] for D_2 in the $3p^3\Pi_u$ state. In these works, several repeated shots at a similar discharge parameter were measured because the spectral window per shot was not enough to measure whole Fulcher-α band emission. In the large helical device (LHD) the ro-vibrational population is measured only up to $v = 2$ and $N = 3$ for H_2 in the $3p^3\Pi_u$ state due to the small spectral window [8, 9]. On the other hand, the ro-vibrational populations up to high N states in the ground state of H_2 and D_2 molecule were recently evaluated by Fulcher-α band spectroscopy for inductively coupled radio-frequency discharge [10]. This method is also applicable for fusion plasmas. In this work, a wide wavelength range Fulcher-α band emission spectroscopy is applied to H_2 and D_2 discharges in LHD, and the populations up to high ro-vibrational states in the ground state are evaluated.

2 Experiment

We selected two discharges for this work, a hydrogen discharge (LHD shot number: #152478) and a deuterium discharge (#150482), the main gas in these discharges being hydrogen and deuterium, respectively. Time traces of the discharge parameters are shown in Figs. 1 and 2 for the hydrogen and deuterium discharges, respectively. Toroidal magnetic field is B_T = 2.64 T in counter-clockwise direction viewed from the top of the torus, and the magnetic axis position is R_{ax} = 3.75 m for both the discharges.

The Fulcher-α band spectra are measured with a wide wavelength range (409-801 nm) high instrumental resolution (~0.07-0.08 nm at 600-630 nm) Echelle spectrometer, developed in our group [11, 12]. In this work, adaptive optics is added in front of the entrance slit. A complementary metal–oxide–semiconductor (CMOS) detector (Andor, Zyla 5.5), having 2560×2160 pixels with the area of 6.5×6.5 μm^2/pixel and 16-bit analog to digital convertors, is used. The viewing area of the spectrometer is on the divertor leg, where the line of sight (LOS) is almost tangential to the magnetic field lines as shown in Fig. 3.

Exposure timings are selected such that the line-averaged electron density in both discharges is not too different; $n_e \approx 6.8 \times 10^{19}$ m^{-3} and $n_e \approx 3.8 \times 10^{19}$ m^{-3} in the hydrogen and deuterium discharges. The central electron temperature in both discharges is $T_e = 1.5 - 3.5$ keV. The plasma parameters along the line of sight (LOS) are calculated with the EMC3-EIRENE code. The calculations show that the most probable emission region of H_2 is near either of the divertor legs. For both discharges the electron temperature near the emission region are $T_e < 10$ eV, and $n_e < 10^{18}$ m^{-3}. The exposure time windows for the spectra collection are 4.80−5.00 s and 3.60−3.70 s for the hydrogen and deuterium discharges, respectively. The raw camera image is converted into the Fulcher-α band spectrum with wavelength and absolute intensity calibrations. The wavelength is calibrated using Th-Ar (Heraeus, P858A) hollow cathode lamp, and a pencil style Hg-Ar and Ne calibration lamps with the precision up to ~0.015 nm [13]. The absolute sensitivity is calibrated with a standard halogen lamp in an integration sphere (Labsphere, USS-600C) placed outside the vacuum chamber.

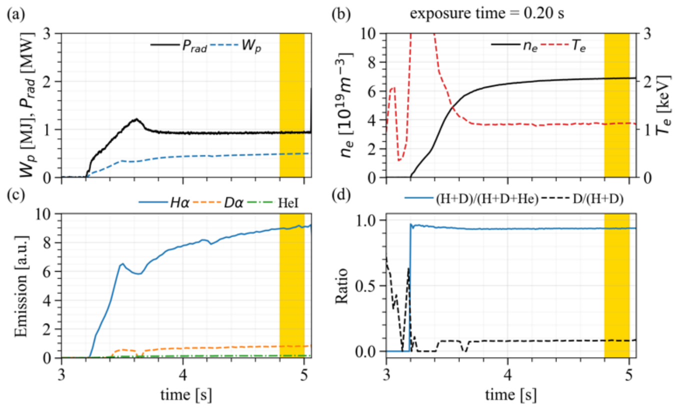

Fig. 1 Time traces of the plasma parameters for the hydrogen discharge (#152478) with indicated exposure time (yellow rectangle). (a) Total radiated power P_{rad} and stored energy W_p, (b) line-averaged electron density n_e and central electron temperature T_e, (c) emission intensities of Hα and Dα, and HeI. (d) density ratio of (H+D)/(H+D+He) [14] and ratio of Dα/(Hα+Dα).

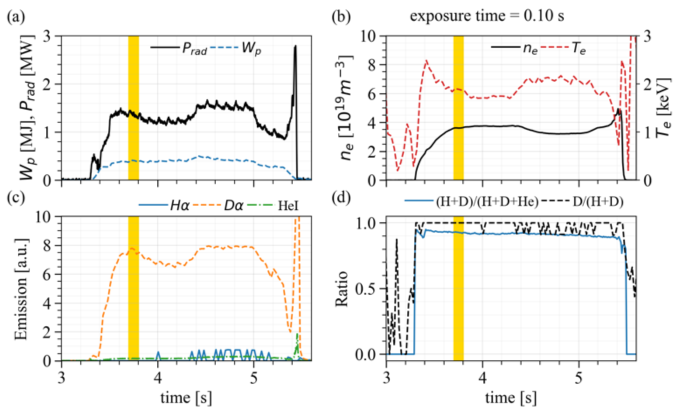

Fig. 2 Time traces of the plasma parameters for the deuterium discharge (#150482) with indicated exposure time (yellow rectangle). (a) Total radiated power P_{rad} and stored energy W_p, (b) line-averaged electron density n_e and central electron temperature T_e, (c) emission intensities of Hα and Dα, and HeI. (d) density ratio of (H+D)/(H+D+He) and ratio of Dα/(Hα+Dα).

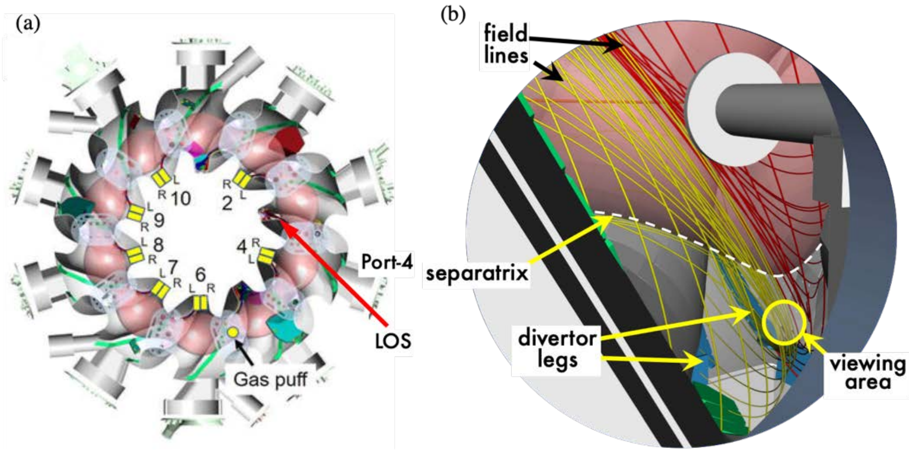

Fig. 3 Line of sight (LOS) of the emission measurement [13]. (a) top view of LHD with LOS shown, (b) view from the port. The viewing area of the spectrometer is on the divertor leg which is shown by blue plates. It is almost tangential to the magnetic field lines which are shown by yellow and red lines.

For the interpretation of the emission region, it is helpful to know the plasma parameters along the LOS. Since there is no available diagnostic to provide such data, plasma parameters along the LOS are calculated with EMC3-EIRENE code. Results for ne and Te are shown in Fig. 4. Note that the coordinates of the left and right divertor legs in the distance along LOS is ~ 3.3m and 4.5 m, respectively.

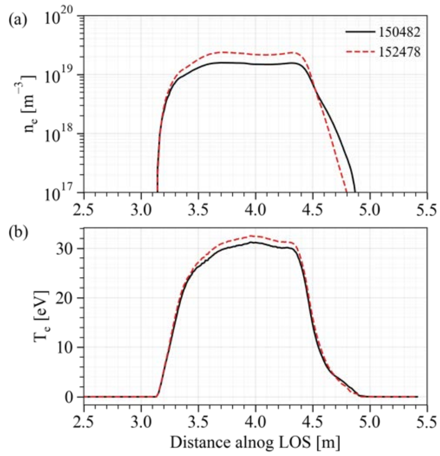

Fig. 4 Plasma parameters along LOS, calculated with EMC3-EIRENE for analyzed discharges 150482 (solid black lines), and 152478 (dashed red lines). (a) electron density n_e, and (b) electron temperature T_e.

3 Results and Discussion

The experimental Fulcher-α band spectra for both selected discharges are shown in Fig. 5. Data from [15, 16] is used for the identification of the Q-branch lines. The spectra are fitted with a single Gaussian or multiple Gaussians, and the spectral area of the single Gaussian or well-separated Gaussians is estimated as the line intensity to be analyzed. An example of line deconvolution is shown in Fig. 6.

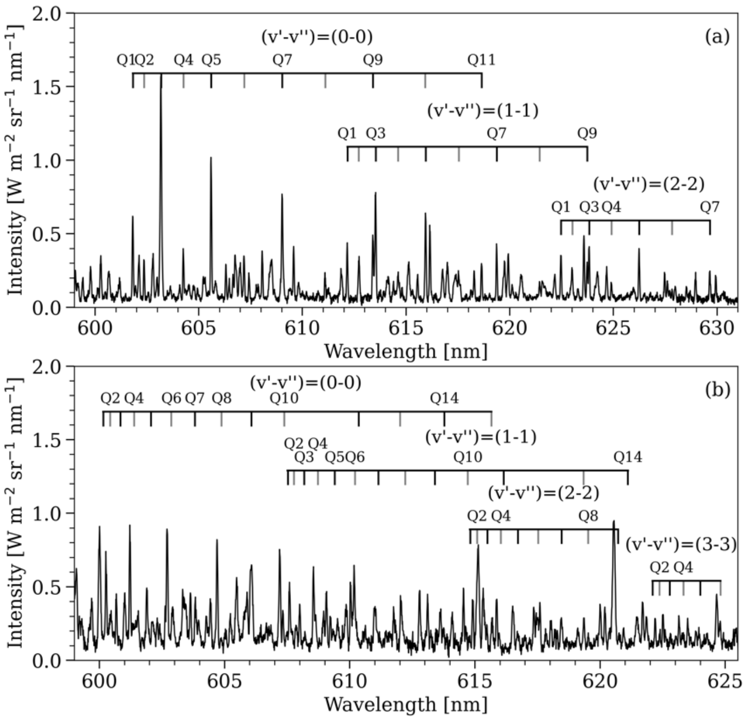

Fig. 5 Observed Fulcher-α band spectra for the hydrogen discharge (a) and the deuterium discharge (b). Q-branch lines used for the intensity analysis are indicated by the Q-branch numbers.

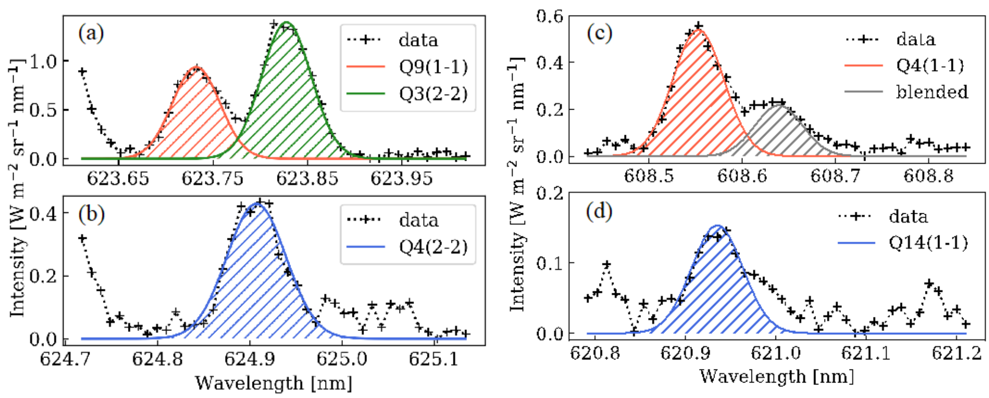

Fig. 6 Examples of Q-branch lines deconvolution. (a), (b) for H_2 discharge, and (c), (d) for D_2 discharge.

In total, 15 and 19 Q-branch lines are used for the hydrogen and deuterium discharges, respectively. List of lines, used for analysis, is summarized in Table 1.

H2						D2					
v'=v"	Q	λ, nm	v'=v"	Q	λ, nm	v'=v"	Q	λ, nm	v'=v"	Q	λ, nm
0	1	601.8299	1	1	612.1787	0	2	600.437	1	4	608.727
0	2	602.3757	1	3	613.5395	0	4	601.391	1	5	609.404
0	4	604.2716	1	7	619.3812	0	6	602.877	1	6	610.213
0	5	607.1996	1	9	623.7457	0	7	603.817	1	10	614.719
0	7	609.0374	2	1	622.4815	0	8	604.882	1	14	621.111
0	9	613.4077	2	3	623.8391	0	10	607.384	2	2	615.089
0	11	618.653	2	4	624.915	0	14	613.786	2	4	616.043
			2	7	629.6622	1	2	607.773	2	8	619.529
						1	3	608.183	3	2	622.379
									3	4	623.331

Table 1. Lines used for analysis. Hydrogen data is from [15] and deuterium from [16].

Relation between the Q-branch line intensities and ro-vibrational populations in the $3p^3\Pi_u$ state, $n_{dv'N'}$, is given as [17, 18]

$$n_{dv'N'} = \frac{I^{dv'N'}_{av''N''}\lambda^{dv'N'}_{av''N''}}{hc}\frac{1}{A^{dv'N'}_{av''N''}} \quad (1),$$

where $I^{dv'N'}_{av''N''}$ is the line intensity, $\frac{\lambda^{dv'N'}_{av''N''}}{hc}$ is the photon energy and $A^{dv'N'}_{av''N''}$ is the radiative emission rate [19]. Here, quantum numbers of upper and lower states of the transition are denoted by $'$ and $''$, respectively.

Boltzmann plots of rotational populations in the $3p^3\Pi_u$ state are shown in Figs. 7 and 8 for every observed vibrational state. As seen in these figures by dashed lines, the rotational population distribution can be well fitted with two-temperature Boltzmann distribution;

$$\frac{n_{dv'N'}}{(2N'+1)g^{N'}_{as}} = \left(1 - a^{v'}\right)\exp\left(-\frac{E^{dv'}_{\mathrm{rot}}(N')}{k_{\mathrm{B}}T^{dv'}_{\mathrm{rot,1}}}\right) + a^{v'}\exp\left(-\frac{E^{dv'}_{\mathrm{rot}}(N')}{k_B T^{dv'}_{\mathrm{rot,2}}}\right) \quad (2).$$

Here $(2N'+1)$ is rotational state multiplicity, $g^{N'}_{as}$ is spin multiplicity, $E^{dv'}_{\mathrm{rot}}(N')$ is rotational energy, k_{B} is the Boltzmann constant. $T^{dv'}_{\mathrm{rot,1}}$ and $T^{dv'}_{\mathrm{rot,2}}$ are rotational temperatures of the low and high temperature component, respectively. $a^{v'}$ is a weighting factor of the high rotational temperature component in the $3p^3\Pi_u$ state [10]. The parameters used for the fitting are listed in Tables 2 and 3 for the hydrogen and deuterium discharges, respectively.

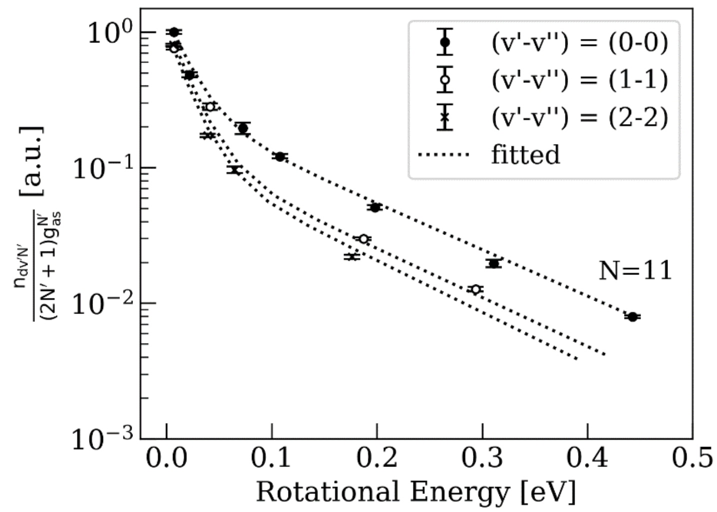

Fig. 7 Rotational energy dependence of the ro-vibrational populations in the $3p^3\Pi_u$ state of H_2 and the fitted result with two-temperature Boltzmann distribution.

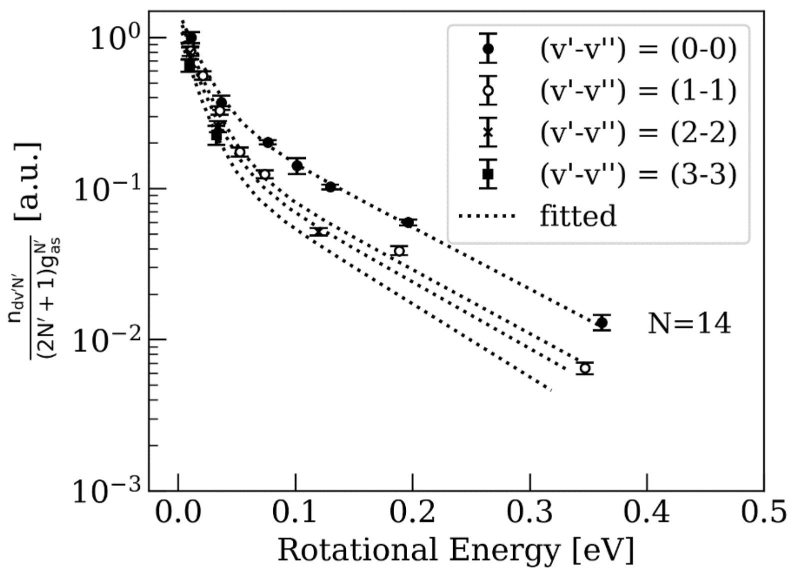

Fig. 8 Rotational energy dependence of the ro-vibrational population in the $3p^3\Pi_u$ state of D_2 and the fitted result with two-temperature Boltzmann distribution.

$T_{\mathrm{rot},1}^{dv'=0}$ (K)	$T_{\mathrm{rot},2}^{dv'=0}$ (K)	$a^{v'=0}$	$a^{v'=1,2}$
240 ± 20	1470 ± 80	0.20 ± 0.04	0.11 ± 0.01

Table 2 Parameters of two-temperature Boltzmann distribution fitting for the $3p^3\Pi_u$ state of H_2.

$T_{\mathrm{rot},1}^{dv'=0}$ (K)	$T_{\mathrm{rot},2}^{dv'=0}$ (K)	$a^{v'=0}$	$a^{v'=1,2,3}$
210 ± 10	1240 ± 40	0.24 ± 0.02	0.14 ± 0.01

Table 3 Parameters of two-temperature Boltzmann distribution fitting for the $3p^3\Pi_u$ state of D_2.

Since vibrational population distribution in the ground state is known to approximately follow a single-temperature Boltzmann distribution up to $v = 4$ [1], we here assume that rotational and vibrational population distributions in the ground state are given as a two-temperature and a single-temperature Boltzmann distribution, respectively. This assumption is expressed as

$$\frac{n_{XvN}}{(2N+1)g_{as}^{N}} = \left[(1-a^{v})\exp\left(-\frac{E_{\mathrm{rot}}^{Xv}(N)}{k_B T_{\mathrm{rot},1}^{Xv}}\right) + a^{v}\exp\left(-\frac{E_{\mathrm{rot}}^{Xv}(N)}{k_B T_{\mathrm{rot},2}^{Xv}}\right)\right]\exp\left(-\frac{E_{\mathrm{vib}}^{X}(v)}{k_B T_{\mathrm{vib}}^{X}}\right) \quad (3),$$

where n_{XvN} is ro-vibrational population, (2*N*+1) is rotational state multiplicity, g_{as}^{N} is spin multiplicity, $E_{\mathrm{rot}}^{Xv}(N)$ is rotational energy, $T_{\mathrm{rot},1}^{Xv}$ and $T_{\mathrm{rot},2}^{Xv}$ are rotational temperatures of low and high temperature components, a^{v} is a weighting factor of high rotational temperature component, $E_{\mathrm{vib}}^{X}(v)$ is vibrational energy, and T_{vib}^{X} is vibrational temperature in the ground state.

A coronal model is used for estimation of the ground state population. We suppose that the coronal model is valid for the present condition of $n_e < 10^{18}$ m^{-3}. The Griem's boundary is higher than 3 for atomic hydrogen. We assume here that this is similar in our case for hydrogen molecule. The coronal model [14, 15] gives the relation between $n_{dv'N'}$ and n_{XvN} with the radiative emission rate and the electron impact excitation rate coefficient, $R_{XvN}^{dv'N'}$, as

$$n_{dv'N'} \sum_{v'',N''} A_{av''N''}^{dv'N'} = n_{\mathrm{e}} \sum_{v,N}\left[n_{XvN} R_{XvN}^{dv'N'}\right] \quad (4).$$

Summation over the rotational quantum numbers in Eq. 4 with Eq. 2 gives a relation of

$$n_{dv'} \sum_{v''=0} A_{av''}^{dv'} = n_{\mathrm{e}} \sum_{v=0}^{2(\mathrm{H_2})\text{ or }3(\mathrm{D_2})}\left[n_{Xv} R_{Xv}^{dv'}\right] \propto \sum_{v=0}^{2(\mathrm{H_2})\text{ or }3(\mathrm{D_2})}\left[R_{Xv}^{dv'}\exp\left(-\frac{E_{\mathrm{vib}}^{X}(v)}{k_B T_{\mathrm{vib}}^{X}}\right)\right] \quad (5),$$

where $n_{dv'}$ is vibrational population in the $3p^3\Pi_u$ state, $A_{av''}^{dv'}$ is the radiative emission rate of vibrational state in the $3p^3\Pi_u$ state, n_{Xv} is vibrational population in the ground state, and $R_{Xv}^{dv'}$ is the electron impact excitation rate coefficient. With Eq. 5, vibrational temperature in the ground state is estimated by a least squares method.

Since it is known that the rotational temperature is proportional to the rotational constant [19], we estimate $T_{\mathrm{rot},1}^{Xv}$ and $T_{\mathrm{rot},2}^{Xv}$ using following relation;

$$T_{\mathrm{rot}}^{Xv} = \frac{B^{Xv}}{B^{dv'}} T_{\mathrm{rot}}^{dv'} \quad (6),$$

where B^{Xv} and $B^{dv'}$ are rotational constants of the ground and $3p^3\Pi_u$ states, respectively. Finally, we determine a^{v} in the ground state assuming diagonal transition for the rotational excitation to be dominant

[10]. The results are shown in Tables 4 and 5 for H_2 and D_2, respectively, and thus estimated ro-vibrational population distributions in the ground state are shown in Figs. 9 and 10 for H_2 and D_2, respectively.

T_{vib}^{X} (K)
9200 ± 600

state	$T_{\mathrm{rot},1}^{Xv}$ (K)	$T_{\mathrm{rot},2}^{Xv}$ (K)	a^{v}
$v = 0$	480 ± 40	3000 ± 150	0.11 ± 0.01
$v = 1$	480 ± 40	2800 ± 150	0.11 ± 0.01
$v = 2$	480 ± 40	2600 ± 140	0.20 ± 0.04

Table 4 (upper) Vibrational temperature, (lower) low and high rotational temperatures, and the weighting factor of the high rotational temperature component at each vibrational state in the ground state of H_2.

T_{vib}^{X} (K)
9600 ± 180

state	$T_{\mathrm{rot},1}^{Xv}$ (K)	$T_{\mathrm{rot},2}^{Xv}$ (K)	a^{v}
$v = 0$	420 ± 30	2480 ± 90	0.14 ± 0.01
$v = 1$	410 ± 30	2390 ± 80	0.14 ± 0.01
$v = 2$	390 ± 30	2300 ± 80	0.24 ± 0.02
$v = 3$	380 ± 30	2210 ± 80	0.24 ± 0.02

Table 5 (upper) Vibrational temperature, (lower) low and high rotational temperatures, and the weighting factor of the high rotational temperature component at each vibrational state in the ground state of D_2.

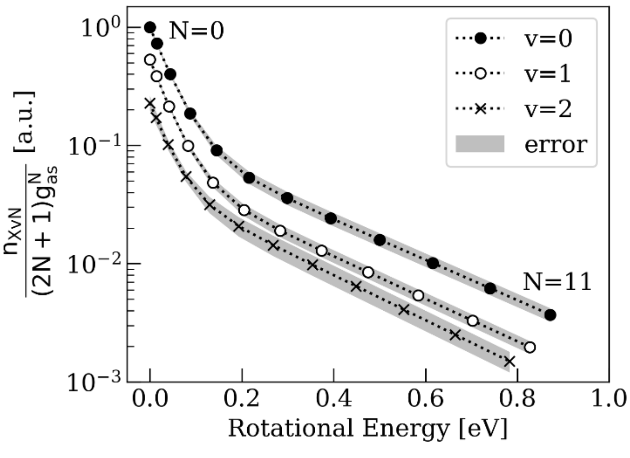

Fig. 9 Rotational energy dependence of the ro-vibrational population in the ground state of H_2.

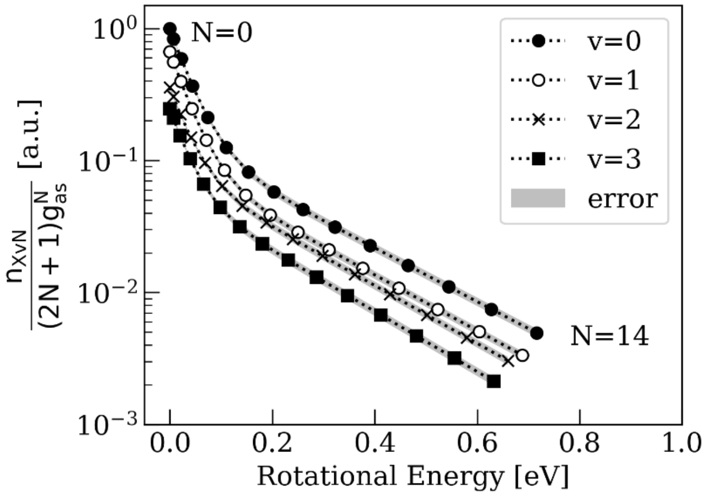

Fig. 10 Rotational energy dependence of the ro-vibrational population in the ground state of D_2.

To confirm the validity of the analysis procedure, the experimental $n_{dv'N'}$ obtained from Eq. 1 and the reconstructed $n_{dv'N'}$ from n_{XvN} in Figs. 7 and 8 with Eq. 4 are compared in Figs. 11 and 12 for H_2 and D_2, respectively. The uncertainty of the experimental $n_{dv'N'}$ comes from Gaussian fitting error for the spectral area estimation, and that of the reconstructed $n_{dv'N'}$ comes from accumulation of the parameter uncertainties in the fitting procedure. The experimental $n_{dv'N'}$ is well reproduced by the reconstructed one.

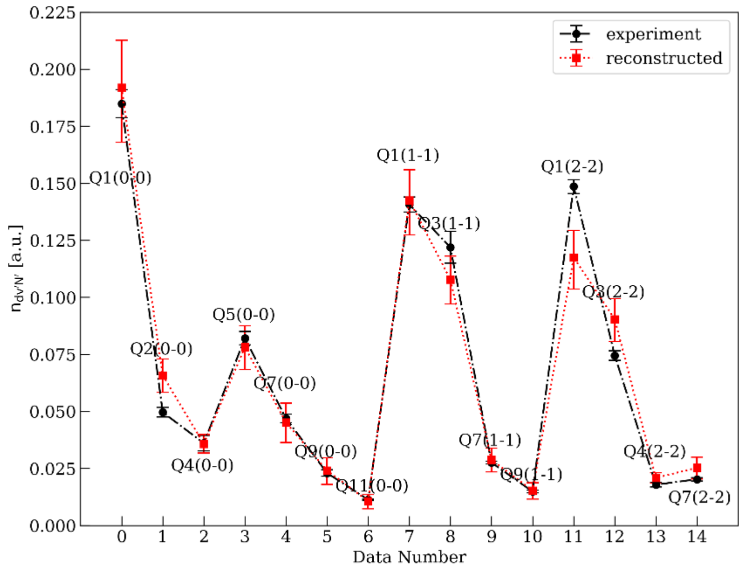

Fig. 11 Comparison of the experimental and reconstructed ro-vibrational populations in the $3p^3\Pi_u$ state of H_2. The horizontal axis shows the data number, and corresponding Q-branch line is indicated by the Q-branch number.

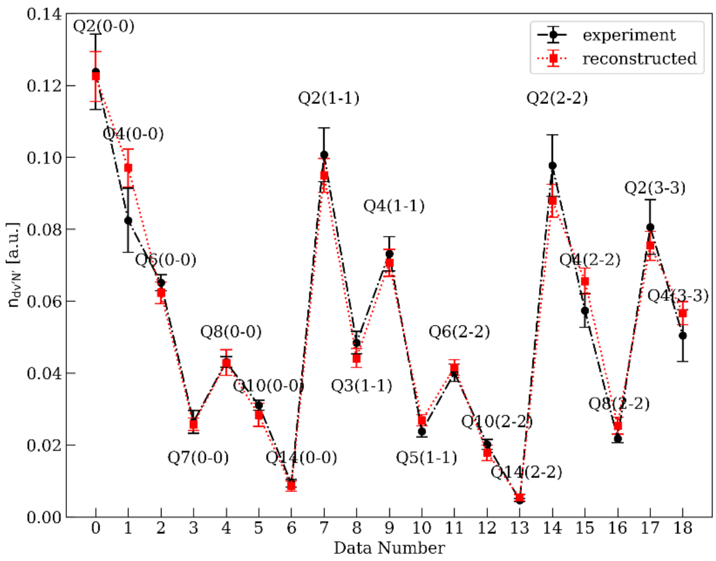

Fig. 12 Comparison of the experimental and reconstructed ro-vibrational populations in the $3p^3\Pi_u$ state of D_2. The horizontal axis shows the data number, and corresponding Q-branch line is indicated by the Q-branch number.

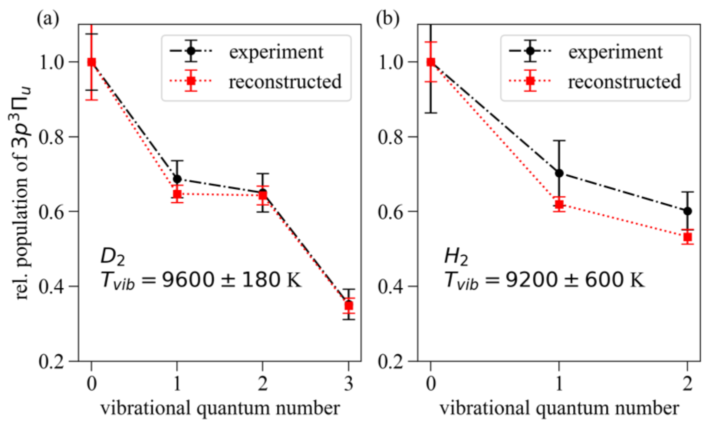

Fig. 13 Relative population of $3p^3\Pi_u$ vibrational levels for (a) D_2, and (b) H_2 discharges.

Fig. 13 displays the behavior of T_{vib} for deuterium (a) and hydrogen (b) discharges. In both cases one can see a good agreement between the experimental data and reconstructed pullulation with T_{vib} = 9600 K and 9200 K for deuterium and hydrogen plasmas, respectively.

Three possible origins of the two-temperature Boltzmann distribution as observed here were discussed in [4]; rotational excitation by electrons, dissociative recombination of H_3^+ and surface association of hydrogen atoms. To identify the main process, further knowledge of plasma parameters in the LHD peripheral region and neutral transport there including MAR processes [20] is a subject for future investigations. Another possibility is that there are two kinds of emission region along LOS with different rotational temperatures. As in [21], the H_2 emission of Q1, 2 lines is peaked in the center of a plasma beam. From [8, 9] it is clear that the H_2 emission regions are located where $n_e \sim 10^{18}$ /m^3 and $T_e \sim 10$ eV and that the position dependence of T_{rot}

estimated from Q1, 2, 3 lines is very small. The actual origin of the observed bi-Boltzmann distribution is not clear.

4 Summary

The ro-vibrational population distributions of H_2 and D_2 in LHD peripheral plasmas were estimated from Fulcher-α Q-branch emission spectra measured with a single shot exposure by a high-resolution echelle spectrometer. From the estimated population distributions with a coronal model, ro-vibrational populations up to v = 2 and N = 11 of H_2 and up to v = 3 and N = 14 of D_2 in the ground state, for the first in LHD plasmas, were deduced. It was found that the rotational population of every vibrational state follows two-temperature Boltzmann distribution.

5 Acknowledgments

This work has been financially supported by the NIFS Collaborative Research Program NIFS16KOAP031 and by Grant-in-Aid for Scientific Research, Nos. 20K20962, and 19H01878 from the Japan Society for the Promotion of Science.

References

[1] K. Sawada and M. Goto, Atoms **4**, 4 (2016).

[2] J. Horacek, *et al.*, NIFS-DATA-73, (2003).

[3] S. Saito, *et al.*, Contrib. Plasma Phys., e201900152 (2020).

[4] P. Vankan, *et al.*, Chem. Phys. Lett. **400**, 196 (2004).

[5] T. Mosbach, *et al.*, Phys. Rev. Lett. **85**, 3420 (2000).

[6] S. Brezinsek, *et al.*, Contrib. Plasma Phys. **42**, 668 (2002).

[7] E.M. Hollmann, *et al.*, Plasma Phys. Control. Fusion. **48**, 1165 (2006).

[8] K.Fujii, *et al.*, Phys. Plasmas **20**, 012514 (2013).

[9] K. Fujii, K. Sawada, *et al.*, Plasma and Fusion Res. **10**, 3402041 (2015).

[10] S. Briefi, *et al.*, J. Quant. Spectrosc. Radiat. Transfer **187**, 135 (2017).

[11] M.Hasuo, K.Fujii, T.Shikama, S.Morita, M.Goto, and H.Tanaka, *J. Phys.: Conf. Ser.*, **397** 012016 (2012)

[12] H. Tanaka, *et al.*, Atoms, **8**(4), 81 (2020)

[13] A. Kuzmin, *et al.*, Plasma and Fusion Res., **13** 3402058 (2018)

[14] M. Goto *et al.*, Physics of Plasmas 10, 1402 (2003)

[15] H. M. Crosswhite, *et al.*, The hydrogen molecule wavelength tables of Gergard Heinrich Dieke (Wiley-Interscience, 1972)

[16] R.S. Freund, *et al.*, J. Phys. Chem. Ref. Data **14**, 235 (1985).

[17] S. Kado, *et al.*, J. Plasma Fusion Res. **80**, 783 (2004).

[18] T. Shikama, *et al.*, J. Plasma Fusion Res. **2**, S1045 (2007).

[19] A. Astashkevich and B.P. Lavrov, J. Quant. Spectrosc. Radiat. Transfer **56**, 725 (1996).

[20] K. Sawada, H. Nakamura, S. Saito, G. Kawamura, M. Kobayashi, K. Haga, T. Sawada, M. Hasuo, Contrib. Plasma Phys., e201900153 (2020).

[21] G. R. A. Akkermans, *et al.*, Phys. Plasmas **27**, 102509 (2020)